Robotica (2010) volume 28, pp. 607–619. © Cambridge University Press 2009
doi:10.1017/S0263574709990282

Investigation of axial forces on dynamic properties of a flexible 3-PRR planar parallel manipulator moving with high speed

Xuping Zhang*, James K. Mills and William L. Cleghorn

Department of Mechanical and Industrial Engineering, University of Toronto, 5 King's College Road, Toronto, Ontario, Canada M5S 3G8

(Received in Final Form: June 24, 2009. First published online: August 11, 2009)

SUMMARY

The effect of axial forces on the dynamic properties is formulated and investigated for a 3-PRR planar parallel manipulator with three flexible intermediate links. A dynamic model of the manipulator system is developed based on the assumed mode method with the consideration of the effect of longitudinal forces on lateral stiffness is included. The flexible intermediate links are modeled as Euler–Bernoulli beams with pinned-pinned boundary conditions, which are verified by experimental modal tests. Natural frequencies of bending vibration of the intermediate links are derived as the functions of axial force and rigid-body motion of the manipulator. Dynamic behavior including the effect of axial forces on lateral deformation is investigated, and configuration-dependant frequencies are analyzed. Numerical simulations of configuration-dependent frequency properties and axial forces are performed to illustrate the effect of axial forces on the dynamic behaviors of the flexible parallel manipulator. Simulation results of mode amplitudes, deformations, axial forces, inertial, and coupling forces are presented, and further validate the theoretical derivations. These analyses and results provide a new and valuable insight to the design and control of the parallel manipulators with flexible intermediate links.

KEYWORDS: Flexible manipulators; Parallel manipulators; Assumed mode method; Dynamic stiffening; Axial force.

1. Introduction

Compared with serial link manipulators with open-loop kinematic chain structure, parallel link manipulators provide higher strength to weight and stiffness to weight ratios, and higher accuracy.[1] Application of parallel link manipulators has increased in various manufacturing industries, i.e., precision optics, nanomanipulation, and medical surgery. Higher productivity demands that manipulators operate with high speed and carry large payloads, while maintaining good positional accuracy. To meet the high-speed requirement, it is desirable to design manipulators with lightweight links in order to decrease the inertia. However, the lightweight links may deflect when the manipulator moves at high speed. The practical solution to this problem is to design and construct lightweight manipulators which are capable of rapid motion, but allow links to deform under high-speed and high-acceleration motions. Then, utilizing dynamic models developed for control system design, undesirable link vibrations may be compensated.[40] Given the advantages of parallel manipulators and lightweight manipulators, a 3-PRR planar parallel manipulator with lightweight intermediate links[2] was developed to provide an alternative high-speed pick-and-place positioning mechanism to serial architecture manipulators, such as X–Y tables or gantry robots. The parallel manipulator presented in this research is shown in Fig. 1. It is categorized as a 3-PRR type because it has three symmetric closed-loop chains, and each of which consists of one prismatic joint (P) and two consecutive revolute joints (R).

Lightweight links are more likely to exhibit structural defection and vibrate due to the inertial forces from high-speed motion, and external forces from actuators. Structural flexibility effects are much more pronounced at high operational speeds and accelerations of the end-effector. Therefore, to provide a direction for the development of an effective vibration control methodology that suppresses these undesired structural vibrations and joint motion control strategies that tracks desired joint trajectories, we must develop a detailed dynamic model to describe the modal characteristics of these structural vibrations as accurately as possible with consideration of the influence of link flexibility of manipulators or mechanisms.

Modeling of multibody dynamics with flexible links is a challenging task and considerable effort has been devoted to the investigation of the dynamic modeling of manipulators and mechanisms with flexible links since the 1970s. Early investigations mainly involved the modeling of flexible serial manipulators and four-bar mechanisms, with detailed reviews by Lowen and Chassapis[3] and Shabana,[4] and recently by Dwivedy and Eberhard.[5] Recently with consideration of link flexibility, Giovagnoni[6] presented a general approach for the dynamic analysis of closed-chain manipulators using the principle of virtual work. Lee and Geng[7] developed a dynamic model of a flexible Stewart platform using Lagrange equations. Fattah *et al.*[8] formulated the dynamic model of a 3-DOF spatial parallel manipulator with flexible links. Zhou *et al.*[9] established dynamic equations of flexible 3PRS manipulator for vibration analysis using FEM. Based on the assumed mode method, Kang and Mills[10] presented a

* Corresponding author. E-mail: zhxp@mie.utoronto.ca

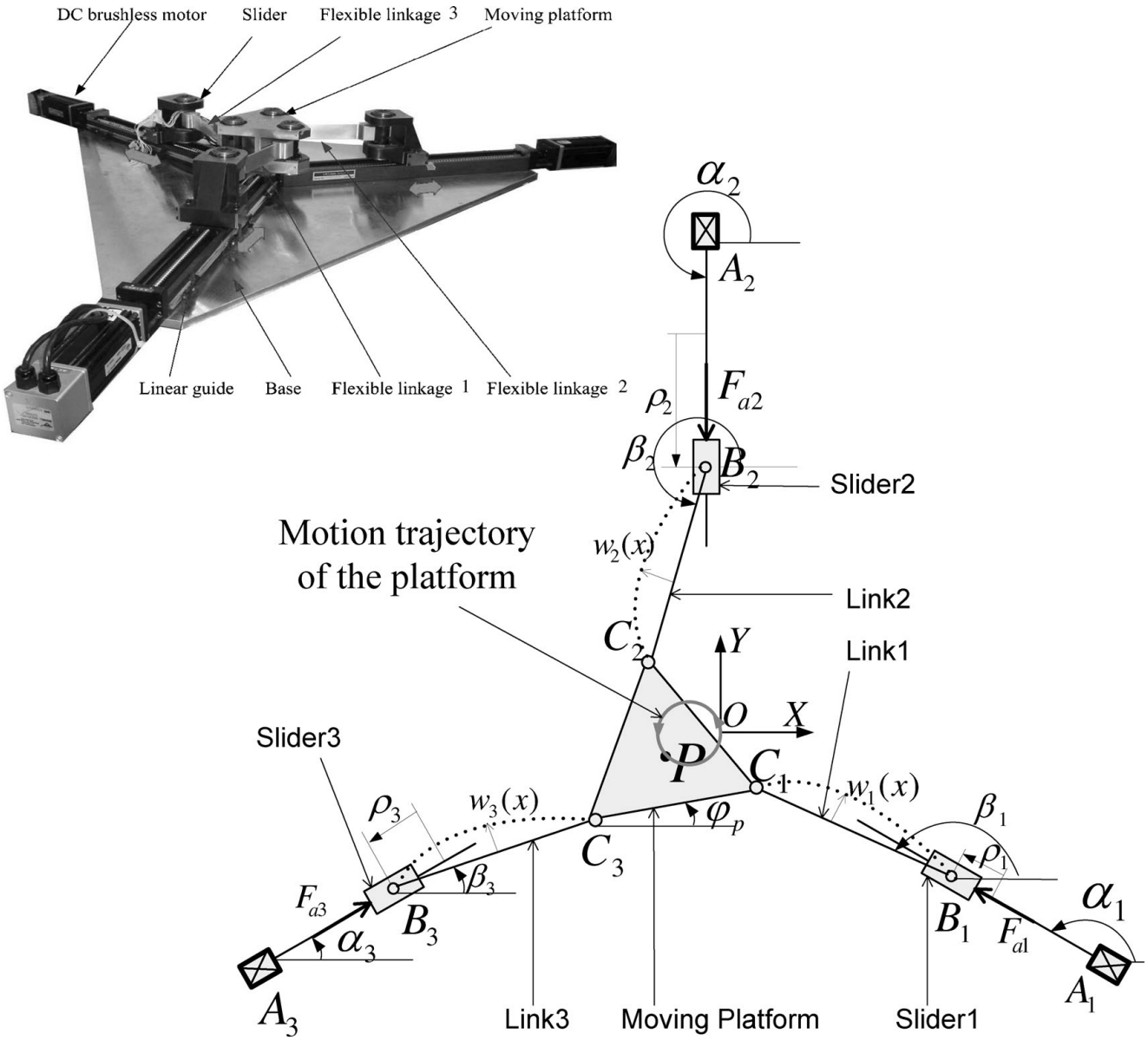

Fig. 1. Architecture and coordinate system of the proposed manipulator.

dynamic model of a 3-PRR planar parallel manipulator with flexible links modeled with pinned-free boundary conditions. Further work[11] including experimental mode verification tests showed that mode properties of the links match pinned-pinned boundary conditions.

Manipulators and mechanisms with link flexibility may be modeled with nonlinear partial differential equations, leading to infinite dimensional models. However, such dynamic equations are cumbersome for both simulation and controller design. Therefore, dynamic modeling formulation of flexible link manipulators and mechanisms has been carried out based on various discretization approaches of flexible links, for example, the finite element method (FEM)[12–17] and the assumed mode method.[18–21] With these discretization approaches, Hamilton's principle or Lagrange equations may be used to develop dynamic equations of flexible manipulators and mechanisms. To model link flexibility, a number of research works employ Euler–Bernoulli beam models assuming that shearing and rotary inertia effects are negligible.[13] Other work has adopted Timoshenko beam models including the effect of shearing and rotary inertia.[22] Dynamic analysis of mechanical systems with link flexibility requires that both gross body motion and concurrent small elastic deformation of flexible links be accounted for, but also includes important coupling effects which exists between rigid body an flexible mode behavior. An important coupling effect, termed geometrical non-linearity, results from the variations in flexible body stiffness induced by inertial forces, internal constraint forces, and external loads. This phenomenon arises under the action of large external loads or during high-speed motion. Typical examples of this behavior are dynamic stiffening (also called stress, geometric, and rotational stiffening). In particular, dynamic stiffening has been investigated for beams undergoing large rotational motion. Kane *et al.*[23] investigated the geometric stiffening of a rotating beam using nonlinear beam theory. Yoo *et al.*[24] established dynamic equations of a beam undergoing overall motions incorporating geometric stiffening. Piedboeuf and

https://doi.org/10.1017/S0263574709990282 Published online by Cambridge University Press

Moore[25] presented six methods of modeling a flexible rotating beam, including geometric stiffening, by taking into account foreshortening in the beam model. Behzad and Bastami[26] studied the effect of axial forces produced by the Poisson effect on the natural frequency of a shaft rotating its longitudinal axis. Liu and Hong[27] put forward a criterion for inclusion of a geometric stiffening term in the motion of a flexible beam using an influence ratio. Since external loading and inertial forces may induce axial forces in beams, several works include the effect of the dynamic stiffening term in modeling lateral deformation of flexible links of manipulators[17] and four-bar mechanisms.[13] Bokaian[28] investigated the relative critical buckling load of a single-span beam with different combinations of free, pinned, clamped, and sliding boundary conditions at both ends of the beam. Several articles on this subject have been published for four-bar mechanisms.[29] However, little work on this subject has been reported for parallel manipulators due to the complicated dynamics. To obtain accurate dynamic equations of manipulators or mechanisms with link flexibility, another important issue is to determine appropriate boundary conditions, and then select the proper sets of modes for problems of elastic beams that undergo large rigid-body displacements. Bellezza *et al.*[30] presented a mathematical model for a flexible slewing beam with a comparison of clamped and pinned boundary conditions at the root end. Low[31] developed an experimental investigation of the boundary condition of slewing beams using a high-speed camera system, and experimental results suggested that exact natural frequencies are intermediate between the clamped and pinned cases. Shabana[32] demonstrated that different sets of mode shapes and natural frequencies associated with different sets of boundary conditions can be used to obtain the same solution provided that the coordinate system is properly selected.

Part of this work, briefly summarized in this paper for continuity of the presentation, was published in ref. [33]. Our preliminary[11] work addressed the dynamic simulation of a 3-PRR parallel manipulator with three flexible links. Note that longitudinal forces on lateral stiffness is not included and investigated in ref. [11]. This paper is mainly concerned with the effect of axial forces on the dynamic properties, providing a thorough investigation of dynamic modeling of a 3-PRR parallel manipulator with three flexible intermediate links. The dynamic equations of the flexible parallel manipulator are developed based the assumed mode method. The flexibility of the manipulator is mainly concentrated in three intermediate links, as the other structural elements are very stiff. The vibration behavior is excited mainly by the driving forces from the motors, the inertial forces, and the reaction forces due to the payload on the moving platform. The intermediate links are modeled as Euler–Bernoulli beams with pinned-pinned boundary conditions. The effect of longitudinal loads on lateral stiffness is investigated considering the high-speed motion of the manipulator. Natural frequencies of bending vibration of intermediate links are derived as the functions of axial force and rigid-body motion of the manipulator. The effect of axial forces on lateral stiffness is investigated and configuration-dependant frequencies are analyzed. Simulation results further verify the theoretical derivations and analysis. These results provide insight to control or optimize the motion of parallel manipulators to increase the stiffness of flexible intermediate links and decrease undesired vibration. For example, for the prescribed end-effector motion, the configurations of a manipulator can be optimized so that the axial forces in the flexible links are in extension to increase the stiffness.

2. Modeling of an Individual Intermediate Flexible Link

2.1. Architecture and coordinate system of the parallel manipulator system

The parallel manipulator presented in this research is categorized as a 3-PRR type, as shown in Fig. 1. It is comprised of three symmetric closed-loop chains, each of which consists of a prismatic joint (P), and two consecutive revolute joints (R). The moving platform, i.e., the end-effector, is of a regular triangle shape ($C_1C_2C_3$). Each active prismatic joint is driven at $A_i, i = 1, 2, 3$ by an Aerotech BM200 DC brushless servo motor with peak torque 3.5 N·m and a ball screw and linear guide mechanism. The ball screw converts the rotation of motors into translational motion of the slider along the linear guide using the ball screw. Revolute joints collocated with the sliders, at $B_i, i = 1, 2, 3$, connect the slider with the intermediate links. The other ends of the links, $C_i, i = 1, 2, 3$ connect the links with the moving platform, which constrains the motion of the links. The coordinate system for the parallel robot is defined with undeformed links, as shown in Fig. 1. The origin of the fixed frame is selected at the center point o of the moving platform when $\alpha_i = \beta_i$. Parameter α_i is the angle at A_i between the X-axis of the fixed frame and the ith linear guide, and $\alpha = [\,\alpha_1\ \alpha_2\ \alpha_3\,] = [\,150^\circ\ 270^\circ\ 30^\circ\,]$. The origin of $\rho_i, i = 1, 2, 3$ is selected at the center of each linear guide. Angle β_i is defined as the angle at B_i between the X-axis of the fixed frame and the ith intermediate link. F_{ai} is the driving force acting on the ith slider.

2.2. Bending vibration modeling of individual link with the assumed mode method

In this work, the structural flexibility of intermediate links is modeled using the assumed mode method. Each intermediate link is treated as an Euler–Bernoulli beam, as the length of each link is much longer than its thickness, and has two rotary joints at the two ends connecting to the platform and a slider. The platform and sliders are designed and built to be much stiffer than the links, and hence are assumed to be rigid. In the assumed mode method, the deflected intermediate links, as shown in Fig. 1 with dotted lines, are modeled by an infinite number of separable harmonic modes. Since the first few modes dominate the dynamics, the modes are truncated to a finite modal series in terms of spatial mode eigen-functions $\psi_{ij}(x)$ and time-varying mode amplitudes $\eta_{ij}(t)$. Note that the proposed parallel manipulator is planar, and therefore the flexural deformations of all three intermediate links are assumed to be transverse in-plane bending. Transverse shear deformations and rotary inertia of each intermediate link are neglected to simplify the dynamic model with the

https://doi.org/10.1017/S0263574709990282 Published online by Cambridge University Press

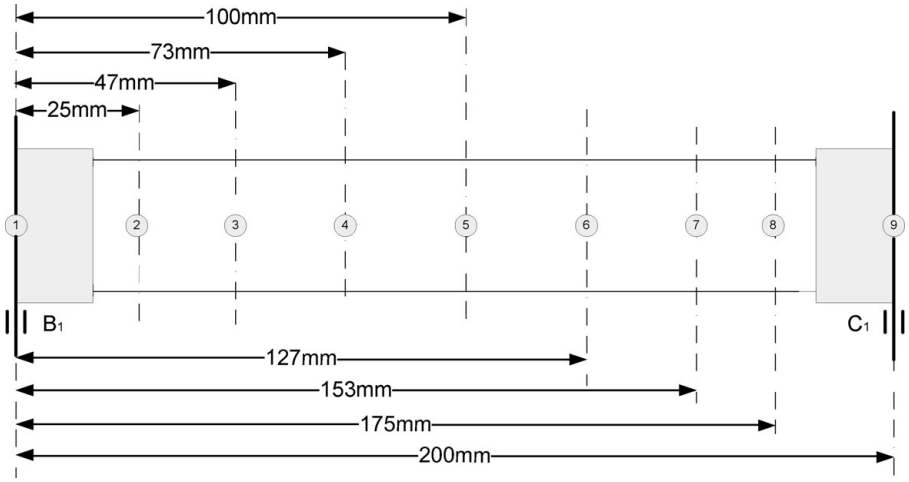

Fig. 2. Location of an accelerometer along the flexible link.

consideration of the fact that that the width is much smaller than the height for each intermediate link. Discussion on the effect of cross-section on the mode shapes can be found in the work by Naguleswaran.[38] The intermediate links are treated as rigid in the longitudinal direction since the axial stiffness of the intermediate links is much higher than the lateral stiffness. The pinned-pinned boundary condition is adopted for the intermediate links based on the modal test results (discussed in Section 2.3), which showed that modal characteristics of the intermediate link match the pinned-pinned boundary condition. Further, we assume that there is no coupling among the modes. The mode coupling issue[39] is not discussed in this work, since the dynamic model is linearized based on the assumed mode method. Therefore, spatial mode shape functions (dependent on x) $\psi_{ij}(\xi)$ are selected as in ref. [34]:

$$\psi_{ij}(x) = \sin(j\pi x/l_i) = \sin(j\pi\xi) = \psi_{ij}(\xi) \quad j = 1, 2, \ldots, r, \tag{1}$$

where $\xi = x/l_i$, r is the number of selected assumed modes, and x is the distance from an arbitrary point on the ith intermediate link to B_i. According to the formulation of the assumed mode method, bending deformation of the ith intermediate link may be expressed as

$$w_i(x,t) = \sum_{j=1}^{r} \eta_{ij}(t)\psi_{ij}(x) \quad i = 1, 2, 3, \tag{2}$$

Flexible generalized coordinates are defined as

$$\bar{\eta} = [\, \eta_{11} \cdots \eta_{1r} \;\; \eta_{21} \cdots \eta_{2r} \;\; \eta_{31} \cdots \eta_{3r} \,]^T \tag{3}$$

where η_{ij} is the jth mode coordinate of the ith intermediate link, $i = 1, 2, 3$, and $j = 1, 2, \ldots, r$.

2.3. *Experimental modal test validation*

To validate the pinned-pinned boundary conditions, experimental modal tests are performed using an impact hammer and an accelerometer to identify the mode shapes of the flexible intermediate links. Detailed modal test results and analyses were provided in our preliminary work found in refs. [2, 11]. During these tests, the three drive motors are locked at their home positions, with the moving platform at the center of the workspace. An impact hammer is used to impact link 1 at point 1, and an accelerometer is fixed to the link sequentially, from points 1–9, as shown in Fig. 2. Using an HP 35670A dynamic response analyzer, with inputs from the hammer and accelerometer, the frequency response function (FRF) at each test location is measured and recorded. At each accelerometer location the average of 15 tests is found. Note that no vibration is measured at both points 1 and 9, as these are the locations of joints B1 and C1. Note also that the vibration at the midpoint position 5 due to the second mode is almost zero. These results coincide with the assumption of pinned-pinned boundary conditions used in the model presented this paper. To further validate the assumed mode shapes in this paper, the measured FRFs are analyzed using experimental modal analysis.[35] The first two mode shapes are derived using the global rational fraction polynomial method, a standard frequency domain modal analysis approach. The first two mode shapes, shown in Figs. 3 and 4, illustrate that the mode shapes from experimental modal tests match very well the mode shapes using in the modeling presented this paper.

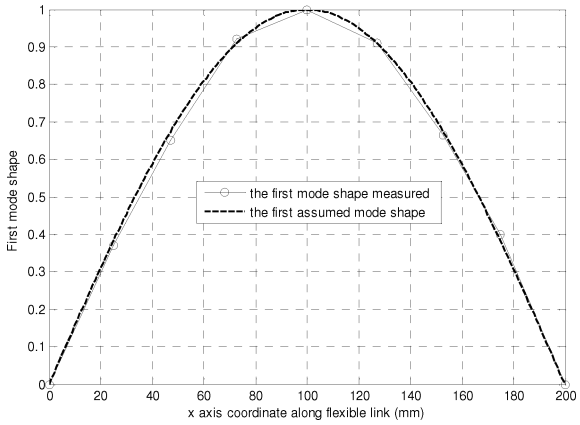

Fig. 3. First mode shape.

https://doi.org/10.1017/S0263574709990282 Published online by Cambridge University Press

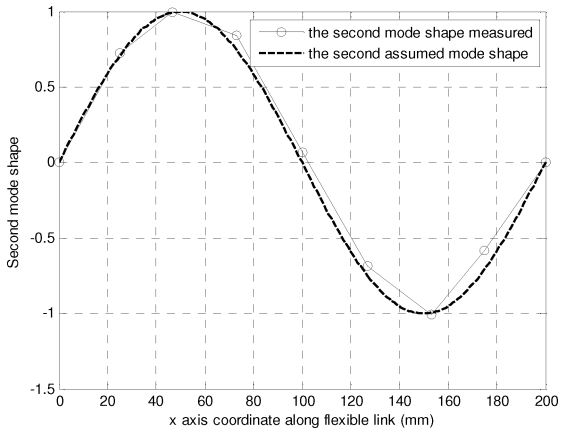

Fig. 4. Second mode shape.

3. Dynamic Equations of Motion for the Manipulator System

In this section, with the consideration of the effect of longitudinal forces on lateral stiffness, the structural dynamic equations of motion of the 3-PRR parallel manipulator with three flexible intermediate links are derived, using the general form of Lagrange's equations. The detailed formulation is below.

3.1. Kinetic energy

The total kinetic energy of the manipulator system includes the kinetic energies of the sliders, intermediate links, and the platform. The kinetic energy of the three sliders is given as

$$T_S = \sum_{i=1}^{3} \frac{1}{2} m_{si} \dot{\rho}_i^2, \tag{4}$$

where m_{si} is mass of the ith slider, and $\dot{\rho}_i$ is the linear velocity of the ith slider.

The kinetic energy of the three intermediate links is expressed as

$$T_L = \sum_{i=1}^{3} \frac{1}{2} \int \rho_{Ai} \left[\dot{\rho}_i^2 + (x\dot{\beta}_i + \dot{w}_i)^2 + 2\dot{\rho}_i (x\dot{\beta}_i + \dot{w}_i) \sin(\alpha_i - \beta_i) \right] \mathrm{d}x, \tag{5}$$

where ρ_{Ai} is mass per unit length of the ith link, $\dot{w}_i$ is the time rate of change of bending deformation of the ith intermediate link, α_i, β_i are defined in Section 2.1, and $\dot{\beta}_i$ is the angular velocity of the ith intermediate link.

In Eq. (5), the nonlinear terms caused by the coupling effect between rigid body motion and elastic deformation are neglected to simplify the model, namely, the model is linearized by noting that the amplitude of the lateral vibrations is small compared to the length of the beam. Therefore, the total motion of the arbitrary point on the flexible intermediate links is the linear superposition of its rigid-body motion and its elastic motion. The kinetic energy of the platform is expressed as

$$T_p = \frac{1}{2} m_p \left(\dot{x}_p^2 + \dot{y}_p^2 \right) + \frac{1}{2} I_p \dot{\varphi}_p^2, \tag{6}$$

where I_p is mass moment of inertia of the platform around the center point P, m_p is the mass of the platform, $\dot{x}_p$ and $\dot{y}_p$ are the linear velocities along X-axis and Y-axis direction, respectively, and $\dot{\varphi}_p$ is the angular velocity of platform.

Therefore, summing the kinetic energies given in Eqs. (4)–(6), the total kinetic energy of the system is:

$$T = \sum_{i=1}^{3} \frac{1}{2} m_{is} \dot{\rho}_i^2 + \sum_{i=1}^{3} \frac{1}{2} \int \rho_{Ai} \left[\dot{\rho}_i^2 + (x\dot{\beta}_i + \dot{w}_i)^2 + 2\dot{\rho}_i (x\dot{\beta}_i + \dot{w}_i) \sin(\alpha_i - \beta_i) \right] \mathrm{d}x + \frac{1}{2} m_p \left(\dot{x}_p^2 + \dot{y}_p^2 \right) + \frac{1}{2} I_p \dot{\varphi}_p^2. \tag{7}$$

3.2. Potential energy

The potential energy of the flexible manipulator system arises from two sources: the elastic deformation of flexible links and gravity. However, since gravitational force is applied along the Z-direction, perpendicular to the X-Y plane, the potential energy due to gravity is not included here.

This work investigates geometric stiffening of intermediate links, specifically, how the longitudinal loads acting on the intermediate links affects the lateral stiffness of the links. Hence, the total potential energy includes the first term: the flexural strain energy, and the second term: the potential energy due to longitudinal loads along the flexible intermediate links undergoing bending deformation. The total potential energy of the system is given as

$$V = \frac{1}{2} \sum_{i=1}^{3} \int E_i I_i (w_i'')^2 \mathrm{d}x + \frac{1}{2} \sum_{i=1}^{3} \int P_{xi}(x) (w_i')^2 \mathrm{d}x = V_1 + V_2, \tag{8}$$

where E_i elastic modulus of the ith link, I_i second area moment of the ith link, load P_{xi} longitudinal loads of the ith link, $w_i' = \frac{\partial w_i(x,t)}{\partial x}$, and $w_i'' = \frac{\partial^2 w_i(x,t)}{\partial x^2}$.

The flexural strain energy can be rewritten as

$$V_1 = \frac{1}{2} \sum_{i=1}^{3} \int E_i I_i \left(\frac{\partial^2 w_i(x)}{\partial x^2} \right)^2 \mathrm{d}x = \frac{1}{2} \sum_{i=1}^{3} \frac{E_i}{l_i^3} \int_0^1 I_i(\xi) \sum_{j=1}^{3} \eta_{ij}^2(t) (\psi_{ij}''(\xi))^2 \mathrm{d}\xi, \tag{9}$$

where ρ_{Ai} is mass per unit length of the ith link, $x = l\xi$, $Hz.$, $0 \le \xi \le 1$ $\psi(x) = \psi(\xi)$, $\frac{\partial \psi(x)}{\partial x} = \frac{\partial \psi(\xi)}{\partial (l\xi)} = \frac{1}{l} \frac{\partial \psi(\xi)}{\partial \xi}$, and $\frac{\partial^2 \psi(x)}{\partial x^2} = \left(\frac{1}{l}\right)^2 \frac{\partial^2 \psi(\xi)}{\partial \xi^2}$. Variable P_{xi} is positive when the longitudinal load is in tension, and P_{xi} is negative when the longitudinal load is in compression.[32]

To derive the potential energy V_2, the longitudinal force P_{xi} in the ith link must be determined. The ith intermediate link and slider are separated from the manipulator system as shown in Fig. 5. The left diagram represents the force analysis of the ith slider, and the right diagram corresponds to the force analysis of the ith intermediate link. F_{ai} is the

https://doi.org/10.1017/S0263574709990282 Published online by Cambridge University Press

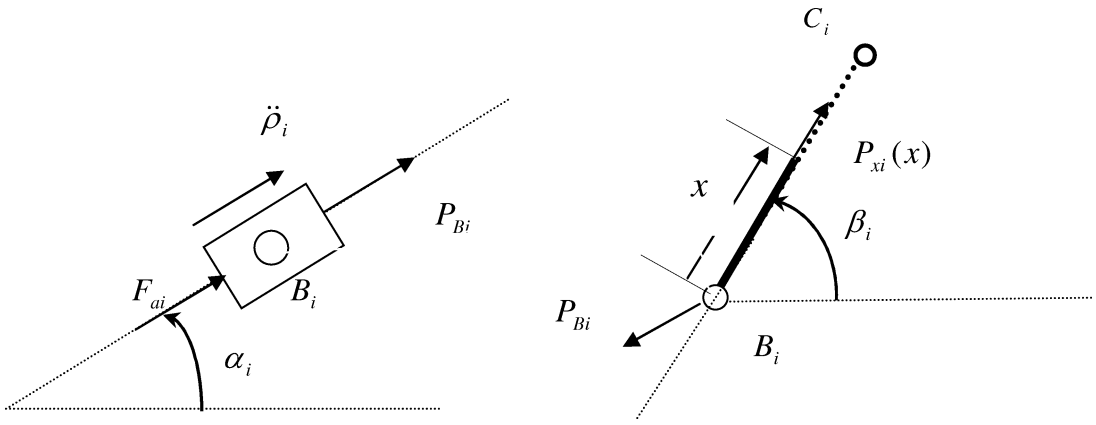

Fig. 5. Force analysis of the ith slider and intermediate link.

driving force applied on the slider ith link, and P_{Bi} is the force applied at the point B_i of the ith link by ith the slider.

The force balance equations of the ith slide and intermediate link can be written as

$$F_{ai} + P_{Bi} = m_{si}\ddot{\rho}_i \tag{10}$$

$$P_{xi} = P_{Bi}\cos(\beta_i - \alpha_i) + \rho_{Ai}\left[\ddot{\rho}_i\cos(\beta_i - \alpha_i)x - \frac{\dot{\beta}_i^2}{2}x^2\right] \tag{11}$$

Then, the axial load applied on the ith intermediate link at the position x is written as

$$P_{xi} = (m_{si}\ddot{\rho}_i - F_{ai})\cos(\beta_i - \alpha_i) + \rho_{Ai}\left[\ddot{\rho}_i\cos(\beta_i - \alpha_i)x - \frac{\dot{\beta}_i^2}{2}x^2\right] \tag{12}$$

Note that the longitudinal deformations are neglected and the transverse deformations are assumed small in this work. Hence, the effect of the shortening of the intermediate links due to lateral deformation on the dynamic behavior is neither derived nor discussed, to simplify the dynamic model, common to much of the literature which addresses structural vibration.[2] Detailed discussions on the effect of shortening projection due to lateral deformation are present in ref. [37].

Equation (9) illustrates that the axial force on the ith intermediate link change with the configuration of the manipulator. This force may be compressive at some configurations, and extensive at others. The analysis of dynamic stiffening will be further discussed in Section 4.

Therefore, the potential energy V_2 in Eq. (8), is given as

$$\begin{aligned} V_2 = {} & \frac{1}{2}\sum_{i=1}^{3}\int_0^{l_i}\left[(m_{si}\ddot{\rho}_i - F_{ai})\cos(\beta_i - \alpha_i)\right. \\ & \left. + \rho_{Ai}\ddot{\rho}_i\cos(\beta_i - \alpha_i)x - \rho_{Ai}\frac{\dot{\beta}^2}{2}x^2\right]\left(\frac{\partial w_i(x)}{\partial x}\right)^2 \mathrm{d}x \\ = {} & \frac{1}{2}\sum_{i=1}^{3}\frac{1}{l_i}(m_{si}\ddot{\rho}_i - F_{ai})\cos(\beta_i - \alpha_i)\int_0^1\sum_{j=1}^{r}\eta_{ij}^2(t)(\psi'_{ij}(\xi))^2\,\mathrm{d}\xi \\ & + \frac{1}{2}\sum_{i=1}^{3}\rho_{Ai}\ddot{\rho}_i\cos(\beta_i - \alpha_i)\int_0^1\xi\sum_{j=1}^{r}\eta_{ij}^2(t)(\psi'_{ij}(\xi))^2\,\mathrm{d}\xi \\ & - \frac{1}{4}\sum_{i=1}^{3}\rho_{Ai}l_i\dot{\beta}^2\int_0^1\xi^2\sum_{j=1}^{r}\eta_{ij}^2(t)(\psi'_{ij}(\xi))^2\,\mathrm{d}\xi. \end{aligned} \tag{13}$$

Equation (9) shows that the flexural stain energy V_1 depends on geometric parameters and material properties of intermediate links, but is not configuration-dependant. In contrast, Eq. (13) illustrates that the potential energy V_2 not only depends on geometric parameters and the material properties of intermediate links, but is also configuration-dependent. Substituting Eqs. (9) and (13) into Eq. (8), the total potential energy of the parallel manipulator with flexible intermediate links may be calculated. Combining the kinetic energy derived in Section 3.1 and the potential energy, the dynamic equations of the flexible parallel manipulator system may be derived using Lagrange's equation.

3.3. *Lagrange's equation*

The generalized coordinates for the manipulator with flexible intermediate links include rigid-body motion generalized coordinates and flexible generalized coordinates. However, this paper focuses on the effect of dynamic stiffening on the vibration characteristics of the manipulator system, and hence the rigid-motion dynamics of the manipulators system is neither derived nor discussed here. It is assumed that the small amplitude, high-frequency structural vibrations of the manipulator have a negligible effect on its rigid-body motion, i.e., we adopt the kineto-elasto-dynamics (KED) assumptions, common to much of the literature which addresses structural vibration.[2] Therefore, the influence of the elastic deformation on the rigid-body motion is neglected, and the equations of motion are solved using the prescribed rigid-body motion. Thus, Lagrange's equations are not formulated for rigid-motion generalized coordinates, only for flexible generalized coordinates of the manipulator system. Therefore, the formulation of Lagrange's equations for the flexible generalized coordinates is provided in detail

https://doi.org/10.1017/S0263574709990282 Published online by Cambridge University Press

below,

$$\frac{\mathrm{d}}{\mathrm{d}t}\left(\frac{\partial(T-V)}{\partial\dot{\eta}_{ij}}\right)-\frac{\partial(T-V)}{\partial\eta_{ij}}=0 \qquad i=1,2,3 \quad j=1,2,\ldots,r. \tag{14}$$

Substituting Eqs. (7) and (8) into Eq. (14), we have

$$\begin{aligned}&\left(m_i\int_0^1\psi_{ij}^2\mathrm{d}\xi\right)\ddot{\eta}_{ij}+\left(\frac{E}{l_i^3}\int_0^1(\psi_{ij}'')^2I_i(\xi)\mathrm{d}\xi\right)\eta_{ij}+\left(\frac{1}{l_i}(m_{si}\ddot{\rho}_i\right.\\&\quad-F_{ai})\cos(\beta_i-\alpha_i)\int_0^1(\psi_{ij}')^2\mathrm{d}\xi+\rho_{Ai}\ddot{\rho}_i\cos(\beta_i-\alpha_i)\\&\quad\times\left.\int_0^1\xi(\psi_{ij}')^2\mathrm{d}\xi-\frac{1}{2}\rho_{Ai}l_i\dot{\beta}^2\int_0^1\xi^2(\psi_{ij}')^2\mathrm{d}\xi\right)\eta_{ij}\\&=-m_i\ddot{\rho}_i\sin(\alpha_i-\beta_i)\int_0^1\psi_{ij}\mathrm{d}\xi-m_il_i\ddot{\beta}_i\int_0^1\psi_{ij}\xi\,\mathrm{d}\xi+m_i\dot{\rho}_i\dot{\beta}_i\\&\quad\cos(\alpha_i-\beta_i)\int_0^1\psi_{ij}\mathrm{d}\xi\qquad i=1,2,3\quad j=1,2,\ldots,r.\end{aligned} \tag{15}$$

Equation (15) can be rewritten in matrix form as

$$M\ddot{\bar{\eta}}+(K_f+K_p)\bar{\eta}=-M_\rho\ddot{\bar{\rho}}-M_\beta\ddot{\bar{\beta}}+F_{fg}, \tag{16}$$

where M is the modal mass matrix of the parallel manipulator system, K_f is the conventional modal stiffness matrix, K_p is the modal stiffness matrix due to the effect of axial forces on lateral stiffness, $-M_\rho\ddot{\bar{\rho}}-M_\beta\ddot{\bar{\beta}}$ is the modal force vector caused by the effect of rigid-body motion on elastic vibration of the flexible links, F_{fg} is the modal force vector from the coupling between rigid-body motion and elastic motion, and $m_i=\rho_{Ai}l_i$ is the mass of the ith intermediate link. Detailed expressions for M, M_ρ, M_β, and F_{fg} are given in the Appendix.

4. Configuration-Dependent Stiffness of Intermediate Links

The axial forces on intermediate links of parallel manipulators become significant due to high-speed motion and high payload. Therefore, the effect of axial forces on lateral stiffness is not negligible. In this section, the analysis of dynamic stiffening of intermediate links is based on properties of the natural frequencies of the parallel manipulator.

4.1. Link mode vibration frequency

From Eq. (16), it is clear that the solution to flexible modal coordinates $\bar{\eta}$ includes two parts: free vibration and forced vibration. The generalized force, i.e., the right-hand side of Eq. (16), has no impact on the modal properties of the elastic deformation of the manipulator, and only affects the vibration amplitude. Therefore, evaluation of the modal characteristics only involves the homogeneous part of Eq. (16), given as

$$M\ddot{\bar{\eta}}+(K_f+K_p)\bar{\eta}=0, \tag{17}$$

where M, K_f, and K_p are diagonal matrices. The equation of motion of the jth mode for the ith intermediate link can be written as

$$m_{ij}\ddot{\bar{\eta}}_{ij}+\left(k_{ij}^f+k_{ij}^p\right)\bar{\eta}_{ij}=0, \tag{18}$$

where

$$m_{ij}=\rho_{Ai}l_i\int\psi_{ij}^2\,\mathrm{d}\xi, \tag{19}$$

$$k_{ij}^f=\frac{E_i}{l_i^3}\int I_i(\xi)\psi_{ij}''^2\,\mathrm{d}\xi, \tag{20}$$

$$\begin{aligned}k_{ij}^p&=\frac{1}{l_i}(m_{si}\ddot{\rho}_i-F_{ai})c_i\int\psi_{ij}'^2\,\mathrm{d}\xi+\rho_{Ai}\ddot{\rho}_ic_i\int\psi_{ij}'^2\xi\,\mathrm{d}\xi\\&\quad-\frac{1}{2}m_i\dot{\beta}^2\int\xi^2\psi_{ij}'^2\,\mathrm{d}\xi=\int_0^{l_i}P_{xi}\psi_{ij}'^2(x)\,\mathrm{d}x.\end{aligned} \tag{21}$$

Then, the natural frequency of the jth mode for the ith intermediate link, f_{ij}, is given as,

$$f_{ij}=\frac{1}{2\pi}\sqrt{\frac{k_{ij}^f+k_{ij}^p}{m_{ij}}}. \tag{22}$$

4.2. Configuration-dependent stiffness

The conventional formulation for the natural frequency of the jth mode for the ith intermediate link, f_{ij}^0, is given by neglecting the effect of longitudinal loads acting on the links, and assuming the cross-section of the ith intermediate link is constant, hence we have

$$f_{ij}^0=\frac{1}{2\pi}\sqrt{\frac{k_{ij}^f}{m_{ij}}}=\frac{\pi}{2}\left(\frac{j}{l_i}\right)^2\sqrt{\frac{E_iI_i}{\rho_{Ai}}}. \tag{23}$$

Equation (23) shows that the conventional natural frequency f_{ij}^0 is a function of geometric parameters l_i and I_i, and material parameters E_i and ρ_{Ai}. Hence, the natural frequency is independent the rigid-body motion of the manipulator system, and therefore doesn't change with the configuration of the manipulator system. The effect of geometric stiffening is clearly shown in Eq. (22) as a result of the potential due to longitudinal loads along the flexible intermediate links undergoing bending deformation. Equations (21) and (22) reveal that the frequency, f_{ij}, is not only a function of l_i, I_i E_i, and ρ_{Ai}, but also a function of rigid-body motion, ρ_i,β_i, and driving forces acting on the sliders, F_{ai}, and axial loads acting on intermediate flexible links, P_{xi}. Therefore, the actual frequency, f_{ij}, is configuration-dependent due to inclusion of the effect of longitudinal forces. From Eq. (22), we also find that the effect of longitudinal forces on f_{ij} increases with the speed and acceleration of the rigid-body motion of the manipulator system. Variable f_{ij} increases (stiffness increases) and leads

https://doi.org/10.1017/S0263574709990282 Published online by Cambridge University Press

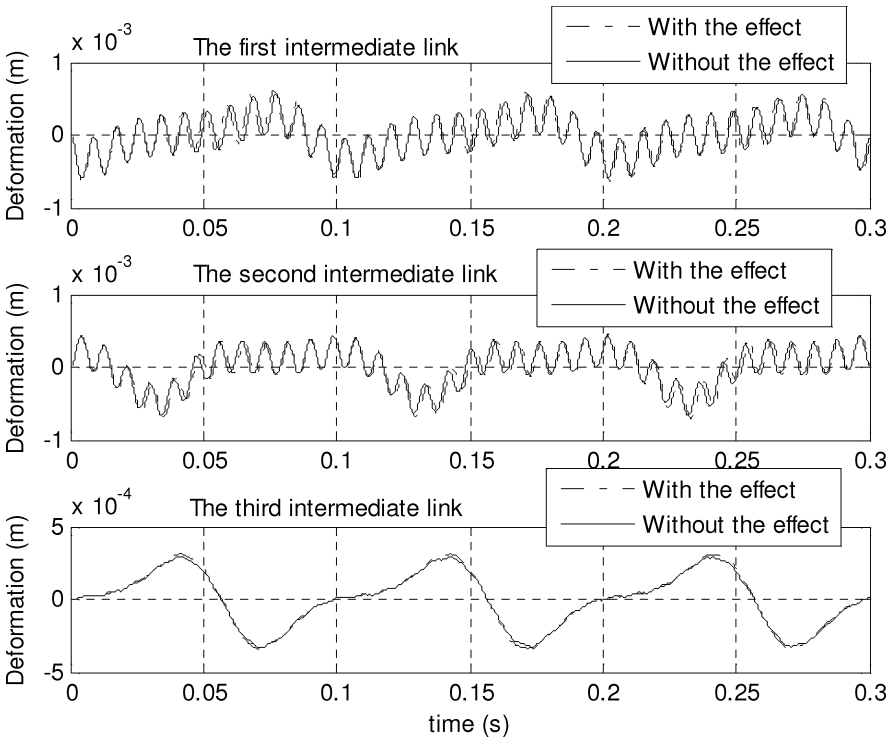

Fig. 6. Deformation of intermediate links when $f = 10$ Hz.

to stiffening when P_{xi} is positive, and decreases (stiffness decreases) and may cause buckling when P_{xi} is negative. The axial forces of intermediate links changes with configuration. They may be in tension at some configurations, and in compression at other configurations. This phenomenon is different than the case of serial manipulators with open-loop structures in which the axial forces are always in extension.

This result provides a mechanism to optimize or control the motion of the manipulator to increase the stiffness of intermediate links and decrease undesired vibration. For example, for the end-effector motion, the configurations of the manipulator may be optimized so that the axial forces in the flexible links are in extension to increase the stiffness. It can be concluded that in the modeling and control of the manipulator with flexible links, the effect of longitudinal loads on lateral stiffness should be included when the manipulator moves with high speed or moves large payloads.

5. Numerical Simulations

Numerical simulations for the 3-PRR parallel manipulator with three flexible intermediate links are presented. In these simulations, a circular motion is used as a desired trajectory for the mass center of the moving platform with constant orientation φ_ρ. The equations for the trajectory are $x_p = 50\cos 2\pi f t - 50(\text{mm})$, $y_p = 50\sin 2\pi f t(\text{mm})$, and $\varphi_\rho = 45^\circ$ constant. Here, f is defined as the frequency of the mass center moving along the described circular trajectory. The intermediate links are modeled as aluminum alloy with Young's modulus and the mass density $E = 7.1 \times 10^{10}\,\text{N/m}^2$, $\rho = 2.77 \times 10^3\,\text{kg/m}^3$, respectively. The three intermediate links have identical geometric parameters. The length of each link is 200 mm, cross-section width 2 mm, and the height of cross-section 30 mm. The distance between adjacent joints on the moving Platform C_iC_j is 100 mm. Linear guides permit a travel range of 400 mm for each slider.

This paper focuses on the study of dynamic stiffening by including the effect of longitudinal loads on lateral vibration frequency properties of the intermediate links. It is assumed that the small amplitude, high-frequency structural vibrations of the manipulator have a negligible effect on the robot rigid-body motion, i.e., we adopt the KED assumptions common to much of the literature which addresses structural vibration. Therefore, the influence of the elastic deformation on the rigid-body motion is neglected to simplify our analysis. Flexible generalized coordinates $\bar{\eta}$ are obtained by solving Eq. (16) using the prescribed rigid-body motion. In the numerical simulations performed, the order of modes retained in the model is selected so that the vibration response of the flexible links from the first order mode is for example, two or three orders of magnitude larger than that of the modes omitted from the reduced order model. We assume that the modes of much higher frequency, omitted from the reduced order model, have little effect on the dynamic behavior of the manipulator system, as they contain little energy. In these simulations, the first three modes are selected to model the structural flexibility of the intermediate links, namely $r = 3$ in Eq. (1). Therefore, flexible generalized coordinates in Eq. (16) are $\bar{\eta} = [\eta_{11}\ \ \eta_{12}\ \ \eta_{13}\ \ \eta_{21}\ \ \eta_{22}\ \ \eta_{23}\ \ \eta_{31}\ \ \eta_{32}\ \ \eta_{33}]^T$. The rigid-body motion of sliders and intermediate links is derived from the given motion of the moving platform by solving the inverse kinematics of the parallel manipulator. Substituting the rigid-body motion into equation (16), the equations become ordinary differential equations (ODEs). With the initial conditions $\bar{\eta} = 0_{9\times1}$, $\bar{\eta} = 0_{9\times1}$, Eq. (16) is solved by MATLAB ODEs solver *ode113* based on a variable order Adams–Bashforth–Moulton method.[36]

Figures 6 and 7 show the bending deformation at the midpoints of intermediate links with $f = 10$ Hz and

https://doi.org/10.1017/S0263574709990282 Published online by Cambridge University Press

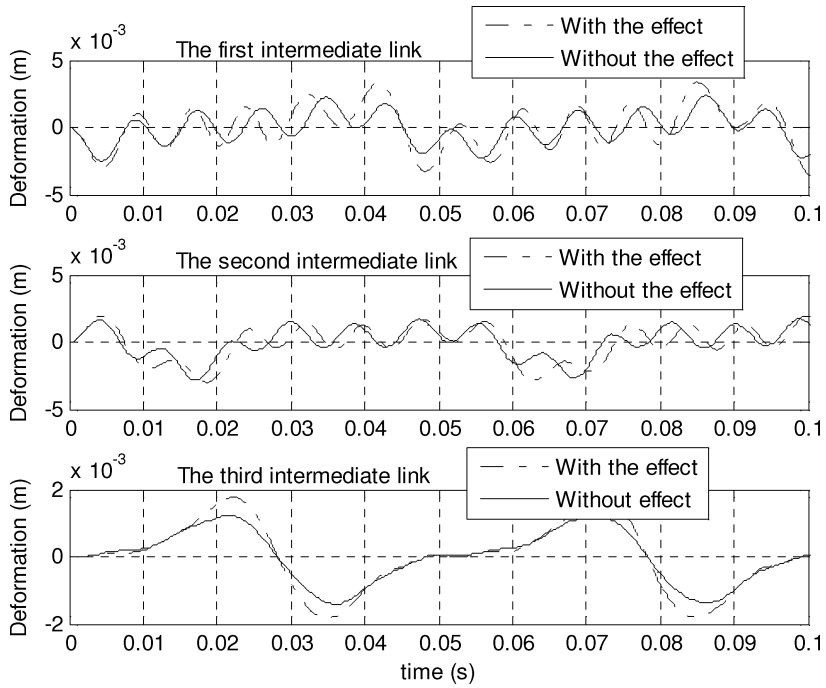

Fig. 7. Deformation of intermediate links when $f = 20$ Hz.

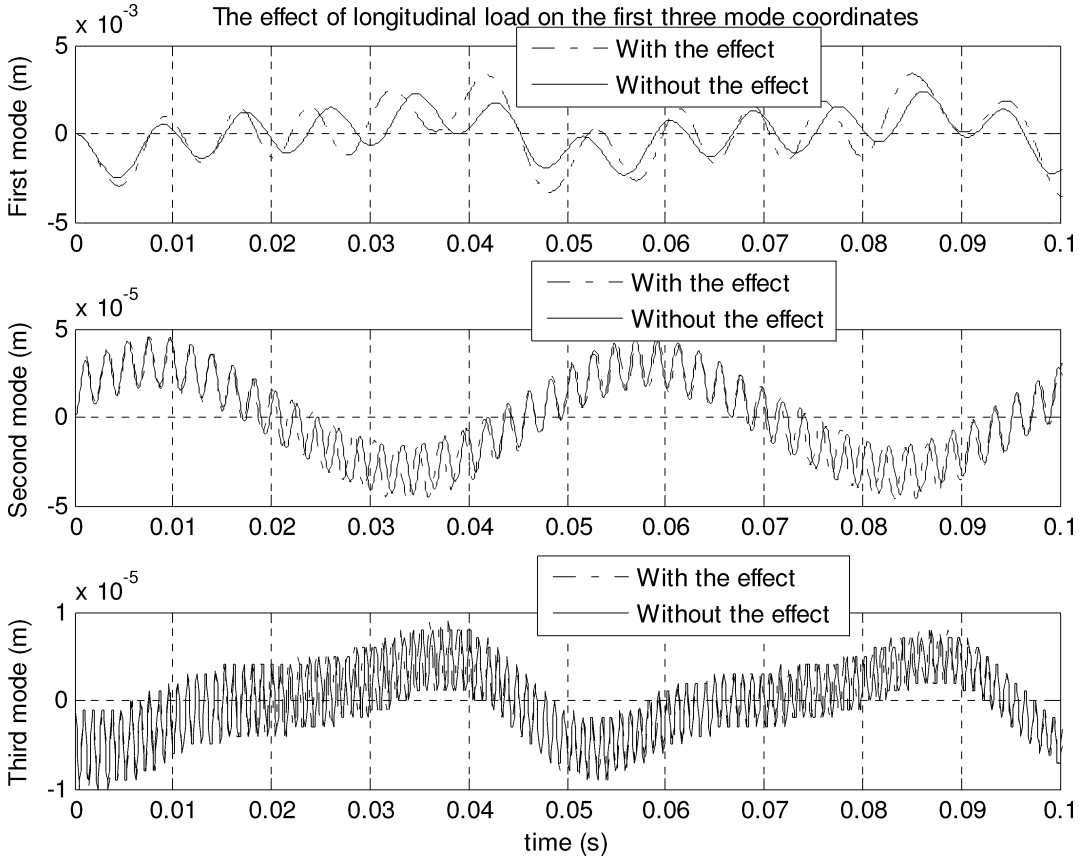

Fig. 8. The first three mode amplitudes when $f = 20$ Hz.

20 Hz, respectively. The effect of axial forces on bending deformation is illustrated in these figures. The effect is not pronounced when $f = 10$ Hz. However, when f increases to 20 Hz, the effect is significant.

Figure 8 reveals that the amplitude of the first mode vibration of the first intermediate link is two magnitudes larger than the amplitude of the second mode vibration. It can be seen that the first mode is sufficiently accurate to describe the vibration of the flexible intermediate link. Therefore, it is reasonable to reduce the number of vibration mode to small finite number. From Fig. 8, it can also be seen that the effect of axial forces on bending deformation decreases with the increase of the number of modes modeled. Figure 10 shows the driving force acting on the first slider required, illustrating

https://doi.org/10.1017/S0263574709990282 Published online by Cambridge University Press

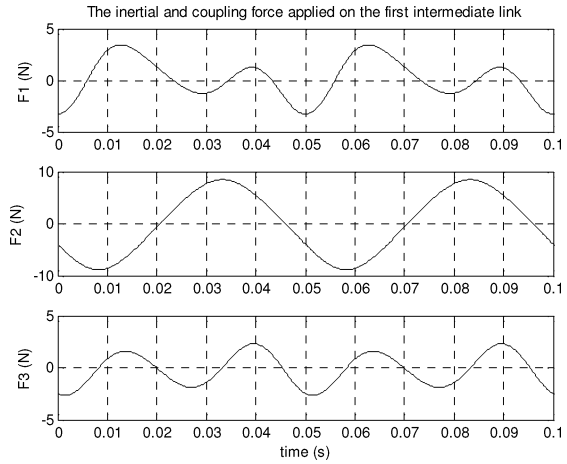

Fig. 9. The inertial and coupling forces when $f = 20$ Hz.

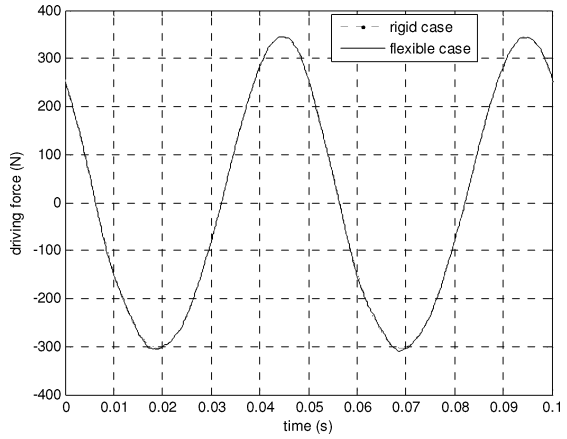

Fig. 10. The driving forces required when $f = 20$ Hz.

the effect of intermediate link flexibility and also the effect of neglecting intermediate link flexibility, respectively. This result illustrates that the driving force corresponding to the two cases is almost the same. The difference is less than 2% as shown in Fig. 11. It is seen that the intermediate link flexibility has little effect on the rigid-body motion of the manipulator system. Therefore, the KED simplification for simulation in this work is justified.

The solution to Eq. (16) includes two parts: free vibration and forced vibration. Without including the effect of longitudinal forces, the *j*th mode frequency of free vibration for the *i*th intermediate link can be written as $f_{ij}^0 = \frac{\pi}{2}\left(\frac{j}{l_i}\right)^2 \sqrt{\frac{E_i I_i}{\rho_{Ai}}}$. Therefore, the first three natural frequencies are calculated to be 116.4 Hz, 465.6 Hz, and 1047.5 Hz. The amplitudes and frequencies of forced

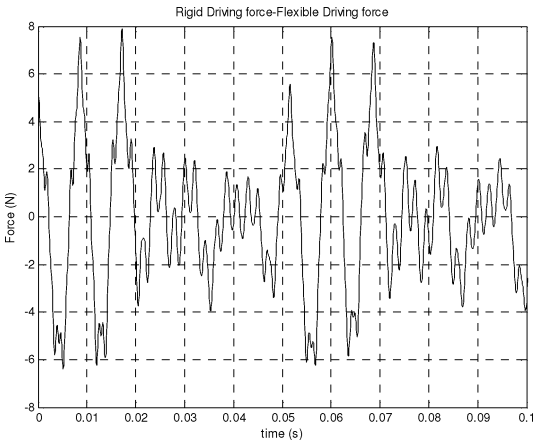

Fig. 11. The difference of driving forces when $f = 20$ Hz.

vibration for the intermediate links are determined by inertial and coupling forces $F_1 = -M_\rho$, $F_2 = -M_\beta$, and $F_3 = F_{fg}$. These inertial and coupling forces are given in Fig. 9 corresponding to the first mode of the first intermediate link with $f = 20$ Hz.

To investigate the dynamic stiffening, Eq. (22) is used to calculate the natural lateral vibration frequencies of the intermediate links. Figures 12–14 compare the first three mode frequencies with the axial force in the first intermediate link. These three figures illustrate clearly the effect of the longitudinal forces on the natural lateral vibration frequencies of the intermediate links. The natural lateral vibration frequencies of the intermediate links exhibit configuration dependency. When the link is in tension, the lateral stiffness increases, and therefore the frequency increases. When the axial force is in compression, the lateral stiffness decreases, and therefore the vibration frequency decreases.

These results provide insight to the control of the motion of the manipulator to increase the stiffness of intermediate links and decrease undesired vibration. For example, for the described end-effector motion, the configurations of the manipulator can be optimized so that the axial forces in the flexible links are in extension to increase the stiffness.

The effect of longitudinal forces on natural frequencies of the first intermediate links is further summarized in Table I. It can be seen that longitudinal forces have a larger effect on flexural vibration for the lower mode frequencies than for the higher mode frequencies. These results are consistent with the theoretical formulation of modal characteristics in Section 4.

The effect of longitudinal forces on natural vibration frequencies of intermediate links becomes paramount with

Table I. The effect of longitudinal force on natural frequencies of the first intermediate link.

	Without the effect of longitudinal force	With the effect of longitudinal force		
		Minimum	Maximum	The change of amplitude
The first mode frequency	116.4 Hz	90.2 Hz	141.3 Hz	44%
The second mode frequency	465.6 Hz	441.7 Hz	492.4 Hz	11%
The third mode frequency	1047.5 Hz	1024 Hz	1075 Hz	5%

https://doi.org/10.1017/S0263574709990282 Published online by Cambridge University Press

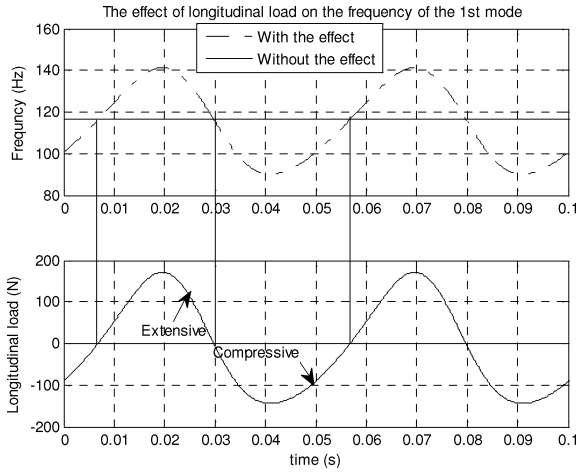

Fig. 12. Axial forces and the first modal frequency when $f = 20$ Hz.

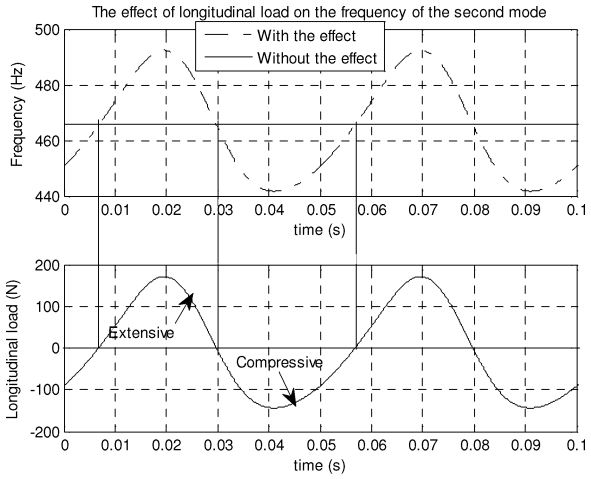

Fig. 13. Axial forces and the second modal frequency when $f = 20$ Hz.

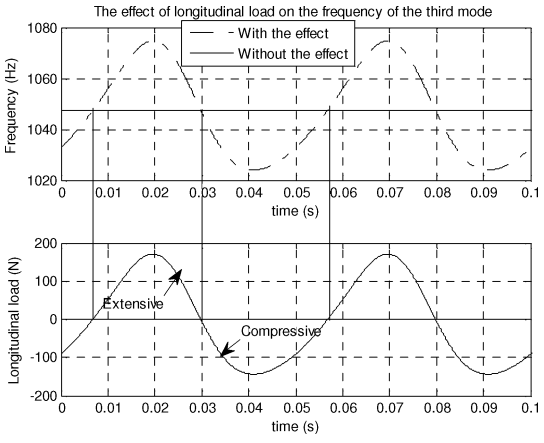

Fig. 14. Axial forces and the third modal frequency when $f = 20$ Hz.

the increase of the speed of rigid-body motion. This is further verified by Fig. 16, which shows the first natural mode frequency change for the first intermediate link corresponding to $f = 10$ Hz, 20 Hz, and 30 Hz The results clearly illustrate that the link natural vibration frequency changes with the configuration of the parallel manipulator,

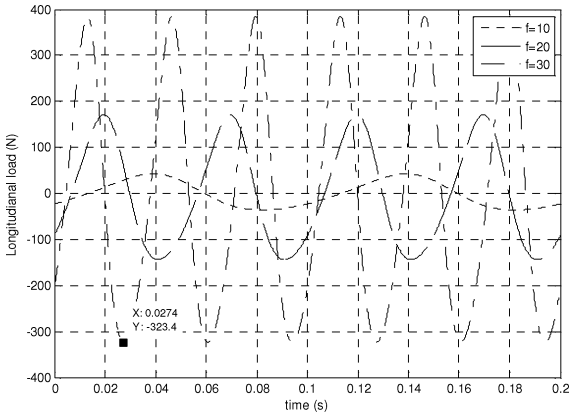

Fig. 15. Axial forces for different *f*.

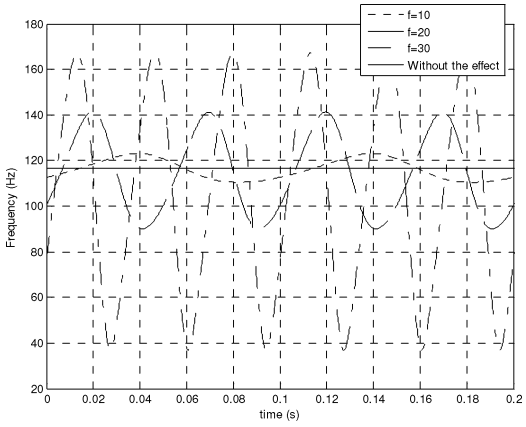

Fig. 16. First mode frequencies change for different *f*.

and the vibration frequency change increases with the speed of the moving platform. The reason for this dynamic behavior is that the axial forces increase with the speed of the manipulator, which is shown in Fig. 15.

To summarize, the effect of longitudinal forces on lateral stiffness should be considered in the design and dynamic simulation when the parallel manipulator moves with high speed. The natural frequencies of flexural vibration for the intermediate links are configuration-dependent and increase with axial forces when axial forces are positive, and decrease when axial forces are negative. Axial forces have a more significant influence on the lower order modal characteristics than on the higher order modal characteristics. The influence increases with increasing speed of rigid-body motion of the manipulator system.

6. Conclusions

In this paper, the effect of longitudinal forces on lateral vibration modal characteristics of a 3-PRR parallel manipulator with three flexible intermediate links has been presented. First, a procedure for the generation of dynamic equations for the parallel manipulator is presented, based on the assumed mode method. The mode shape functions are selected by modeling intermediate links as Euler–Bernoulli beams with pinned-pinned boundary conditions verified by modal experimental tests. The effect of longitudinal forces on lateral stiffness is included in this dynamic

https://doi.org/10.1017/S0263574709990282 Published online by Cambridge University Press

model. Then, the natural frequencies of flexural vibration of intermediate links are derived as the functions of axial force and rigid-body motion during high-speed motion. The mode frequencies indicate both stiffening and buckling by analyzing the effect of longitudinal forces on lateral stiffness and configuration-dependent frequency property. Finally, numerical simulations validate the theoretical analysis and derivation on the modal characteristics and the dynamic stiffening and buckling of intermediate links.

Theoretical derivation and simulation results provide a valuable insight to the design and control of parallel manipulator with flexible intermediate links. It can be concluded that in the modeling and control of parallel manipulators with flexible intermediate links, the effect of longitudinal loads on lateral stiffness should be included when the manipulator moves with high speed or experiences large payloads. The motion of parallel manipulators can be optimized and controlled to increase the stiffness of intermediate links and decrease undesired vibration. For example, for the end-effector motion examined in this work, the configuration of the manipulator may be optimized so that the axial forces in the flexible links are in extension to increase the stiffness. Geometric parameters of intermediate links, payload, and motion velocity and acceleration should be determined according to buckling conditions in the design and dynamic modeling of the parallel manipulator with flexible intermediate links.

Appendix

$$M = \begin{bmatrix} \hat{M}_1 & 0 & 0 \\ 0 & \hat{M}_2 & 0 \\ 0 & 0 & \hat{M}_3 \end{bmatrix} \in R^{3r\times 3r}$$

$$\hat{M}_i = m_i \begin{bmatrix} \int \psi_{i1}^2 d\xi & \cdots & 0 \\ \vdots & \cdots & \vdots \\ 0 & \cdots & \int \psi_{ir}^2 d\xi \end{bmatrix} \in R^{r\times r}$$

$$K_f = \begin{bmatrix} \hat{K}_1^f & 0 & 0 \\ 0 & \hat{K}_2^f & 0 \\ 0 & 0 & \hat{K}_3^f \end{bmatrix} \in R^{3r\times 3r}$$

$$\hat{K}_i^f = \frac{E_i}{l_i^3} \begin{bmatrix} \int I_i(\xi)\psi_{i1}''^2 d\xi & \cdots & 0 \\ \vdots & \cdots & \vdots \\ 0 & \cdots & \int I_i(\xi)\psi_{ir}''^2 d\xi \end{bmatrix} \in R^{r\times r}$$

$$K_p = \begin{bmatrix} \hat{K}_1^p & 0 & 0 \\ 0 & \hat{K}_2^p & 0 \\ 0 & 0 & \hat{K}_3^p \end{bmatrix} \in R^{3r\times 3r}$$

$$\hat{K}_i^p = \begin{bmatrix} \hat{k}_{i1}^p & \cdots & 0 \\ \vdots & \cdots & \vdots \\ 0 & \cdots & \hat{k}_{ir}^p \end{bmatrix} \in R^{r\times r}$$

$$\hat{k}_{ir}^p = \frac{1}{l_i}(m_{si}\ddot{\rho}_i - F_{ai})c_i \int \psi_{ir}'^2 d\xi + \rho_{Ai}\ddot{\rho}_i c_i \int \psi_{ir}'^2 \xi d\xi - \frac{1}{2} m_i \dot{\beta}^2 \int \xi^2 \psi_{ir}'^2 d\xi$$

$$M_\rho = \begin{bmatrix} m_1 s_1 \int \psi_1 d\xi & \cdots & m_1 s_1 \int \psi_r d\xi & 0 & \cdots & 0 & 0 & \cdots & 0 \\ 0 & \cdots & 0 & m_2 s_2 \int \psi_1 d\xi & \cdots & m_2 s_2 \int \psi_r d\xi & 0 & \cdots & 0 \\ 0 & \cdots & 0 & 0 & \cdots & 0 & m_3 s_3 \int \psi_1 d\xi & \cdots & m_3 s_3 \int \psi_r d\xi \end{bmatrix}^T$$

$$M_\beta = \begin{bmatrix} m_1 l_1 \int \psi_{11} \xi d\xi & \cdots & m_1 l_1 \int \psi_{1r} \xi d\xi & 0 & \cdots & 0 & 0 & \cdots & 0 \\ 0 & \cdots & 0 & m_2 l_2 \int \psi_{21} \xi d\xi & \cdots & m_2 l_2 \int \psi_{2r} \xi d\xi & 0 & \cdots & 0 \\ 0 & \cdots & 0 & 0 & \cdots & 0 & m_3 l_3 \int \psi_{31} \xi d\xi & \cdots & m_3 l_3 \int \psi_{3r} \xi d\xi \end{bmatrix}^T$$

$$F_{fg} = \begin{bmatrix} m_1 c_1 \dot{\rho}_1 \dot{\beta}_1 \int \psi_1 d\xi \\ \vdots \\ m_1 c_1 \dot{\rho}_1 \dot{\beta}_1 \int \psi_r d\xi \\ m_2 c_2 \dot{\rho}_2 \dot{\beta}_2 \int \psi_1 d\xi \\ \vdots \\ m_2 c_2 \dot{\rho}_2 \dot{\beta}_2 \int \psi_r d\xi \\ m_3 c_3 \dot{\rho}_3 \dot{\beta}_3 \int \psi_1 d\xi \\ \vdots \\ m_3 c_3 \dot{\rho}_3 \dot{\beta}_3 \int \psi_r d\xi \end{bmatrix}$$

where $s_i = \sin(\alpha_i - \beta_i)$ and $c_i = \cos(\alpha_i - \beta_i)$.

References

1. B. Dasgupta and T. S. Mruthyunjaya, "The Stewart platform manipulator: A review," *Mech. Mach. Theory* **35**, 25–40 (2000).
2. X. Wang and J. K. Mills, "Experimental Modal Analysis of Flexible Linkages in a Smart Parallel Platform," *Proceeding of the 7*th *CANSMART Meeting – International Workshop on Smart Materials and Structures*, Montreal, Canada (2004) pp. 37–46.
3. G. G. Lowen and C. Chassapis, "The elastic behavior of linkage: An update," *Mech. Mach. Theory* **21**(1), 33–42 (1986).
4. A. A. Shabana, "Flexible multibody dynamics: review of past and recent developments," *Multibody Syst. Dyn.* **1**, 189–222 (1997).
5. S. K. Dwivedy and P. Eberhard, "Dynamic analysis of flexible manipulators, a literature review," *Mech. Mach. Theory* **41**, 749–777 (2006).
6. M. Giovagnoni, "Dynamics of flexible closed-chain manipulator," *ASME Des. Tech. Conf.* **69**(2), 483–490 (1992).
7. J. D. Lee and Z. Geng, "Dynamic model of a flexible Stewart platform," *Comput. Struct.* **48**(3), 367–374 (1993).
8. A. Fattah, J. Angeles and A. K. Misra, "Dynamics of a 3-DOF Spatial Parallel Manipulator with Flexible Links," *Proceedings*

https://doi.org/10.1017/S0263574709990282 Published online by Cambridge University Press

of IEEE International Conference of Robotics and Automation, Nagoya, Japan (1995) pp. 274–632.
9. Z. Zhou, J. Xi and C. K. Mechefske, "Modeling of a fully flexible 3PRS manipulator for vibration analsysis," *J. Mech. Des.* **128**, 403–412 (2006).
10. B. S. Kang and J. K. Mills, "Dynamic modeling of structurally-flexible planar parallel manipulator," *Robotica* **20**(3), 329–339 (2002).
11. X. Zhang, J. K. Mills and W. L. Cleghorn, "Dynamic modeling and experimental validation of a 3-PRR parallel manipulator with flexible intermediate links," *J. Intell. Robot. Syst.* **50**, 323–340 (2007).
12. W. Sunada and S.Dubowsky, "The application of the finite element methods to the dynamic analysis of flexible spatial and co-planar linkage systems," *ASME J. Mech. Des.* **103**(3), 643–651 (1981).
13. W. L. Cleghorn, R. G. Fenton and B.Tabarrok, "Finite element analysis of high-speed flexible mechanisms," *Mech. Mach. Theory* **16**, 407–424 (1981).
14. B. S. Thompson and C. K. Sung, "A variational formulation for the nonlinear finite element analysis of flexible linkages: Theory, implementation and experimental results," *ASME J. Mech. Trans. Autom. Des.* **106**, 482–488 (1984).
15. E. Bayo, "A fininte element approach to control the end-point motion of single-link flexible robot," *J. Robot. Syst.* **4**(1), 63–75 (1987).
16. G. Naganathan and A. H. Soni, "Coupling effects of kinematics and flexibility in manipulators," *Int. J. Robot. Res.* **6**(1), 75–85 (1987).
17. Z. Yang and J. P. Sadler, "Large-displacement finite element analysis of flexible linkages," *ASME J. Mech. Des.* **112**, 175–182, (1990).
18. Book W. J., "Recursive Lagrangian dynamics of fexible manipulator arms," *Int. J. Robot. Res.* **3**(3), 87–101 (1984).
19. H. Asada, Z.-D. Ma and H. Tokumaru, "Inverse dynamics of flexible robot arms: Modeling and computation for trajectory control," *ASME. J. Dyn. Sys. Meas. Control* **112**, 177–185 (1990).
20. R. J. Theodore and A. Ghosal, "Comparison of the assumed modes and finite element models for flexible multi-link manipulators," *Int. J. Robot. Res.* **14**, 91–111, (1995).
21. M. H. Korayem, A. Nikoobin and V. Azimirad, "Trajectory optimization of flexible link manipulators in point-to-point motion," *Robotica* (2008). doi: 10.1017/S0263574708005183.
22. J. K. Meek and H. Liu, "Nonlinear dynamics analysis of flexible beams under large overall motions and the flexible manipulator simulation," *Comput. Struct.* **56**(1), 1–14, (1995).
23. T. R. Kane, R. R. Ryan and A. K. Banerjee, "Dynamics of cantilever beam attached to a moving base," *J. Guid. Control Dyn.* **10**, 139–150 (1987).
24. H. H. Yoo, R. R. Ryan and R. A. Scott, "Dynamics of flexible beams undergoing overall motions," *J. Sound Vib.* **181**(2), 261–278 (1995).
25. J. Pieboeuf and B. Moore, "On the foreshortening effects of a rotating flexible beam suing different methods," *Mech. Based Des. Struct. Mach.* **30**(1), 83–102 (2002).
26. M. Behzad and A. R. Bastam, "Effect of centrifugal force on natural frequency of lateral vibration of rotation shafts," *J. Sound Vib.* **274**(3–5), 985–995 (2004).
27. J. Y. Liu and J. Z. Hong, "Dynamics of three-dimensional beams undergoing large overall motion," *Eur. J. Mech. – A/Solids* **23**(6), 1051–1068 (2004).
28. A. Bokaian, "Natural frequencies of beams under compressive axial loads," *J. Sound Vib.* **126**(1), 49–65 (1988).
29. S. W. Gong, "Perfectly flexible mechanism and integrated mechanism system design," *Mech. Mach. Theory* **39**, 1155–1174 (2004).
30. F. Bellezza, L. Lanari and G. Ulivi, "Exact Modeling of the Flexible Slewing Link," *Proceedings of the IEEE International Conference on Robotics and Automation,* Cincinnati, Ohio (1990) pp. 734–739.
31. K. H. Low and M. W. S. Lau, "Experimental investigation of the boundary condition of slewing beams using a high-speed camera system," *Mech. Mach. Theory* **30**, 629–643 (1995).
32. A. A. Shabana, "Resonance conditions and deformable body co-ordinate systems," *J. Sound Vib.* **192**, 389–398 (1996).
33. X. Zhang, J. K. Mills and W. L. Cleghorn, "Effect of Axial Forces on Lateral Stiffness of a Flexible 3-PRR Parallel Manipulator Moving with Hight-Speed," *IEEE International Conference on Information and Automation*, Hunan, China (2008) pp. 1458–1463.
34. S. S. Rao, *Mechanical Vibrations*, 4th ed. (Addison-Wesley, Reading, Massachusetts, 2006).
35. D. J. Ewins, *Modal Testing: Theory, Practice and Application*, 2nd ed. (Research Studies Press, New York, 2000).
36. Solve initial value problems for ordinary differential equations (ODEs), MATLAB Function Reference, The Math Works, Inc. 1994–2005.
37. V. Radisavljevic and H. Baruh, "A comparison of shortening of the projection to axial elasticity," *J. Sound Vib.* **276**, 81–103 (2004).
38. S. Naguleswaran, "Vibration of an Euler–Bernoulli stepped beam carrying a non-symmetrical rigid body at the step," *J. Sound Vib.* **271**, 1121–1132 (2004).
39. S. R. Chen, C. S. Cai, C. C. Chang and M. Gu, "Modal coupling assessment and approximated prediction of coupled multimode wind vibration of long-span bridges," *J. Wind Eng. Ind. Aerodyn.* **92**, 393–412 (2004).
40. Z. Mohamed, A. K. Chee, A. W. I. Mohd Hashim, M. O. Tokhi, S. H. M. Amin and R. Mamat, "Techniques for vibration control of a flexible robot manipulator," *Robotica* **24**, 499–511 (2006).